

Excitation mechanism and thermal emission quenching of Tb ions in silicon rich silicon oxide thin films grown by plasma-enhanced chemical vapour deposition—Do we need silicon nanoclusters?

A. Podhorodecki, L. W. Golacki, G. Zatryb, J. Misiewicz, J. Wang, W. Jadwisienczak, K. Fedus, J. Wojcik, P. R. J. Wilson, and P. Mascher

Citation: *Journal of Applied Physics* **115**, 143510 (2014); doi: 10.1063/1.4871015

View online: <http://dx.doi.org/10.1063/1.4871015>

View Table of Contents: <http://scitation.aip.org/content/aip/journal/jap/115/14?ver=pdfcov>

Published by the *AIP Publishing*

Articles you may be interested in

[Low-temperature electron cyclotron resonance plasma-enhanced chemical-vapor deposition silicon dioxide as gate insulator for polycrystalline silicon thin-film transistors](#)

J. Vac. Sci. Technol. A **24**, 280 (2006); 10.1116/1.2167971

[Composition, structural, and electrical properties of fluorinated silicon–nitride thin films grown by remote plasma-enhanced chemical-vapor deposition from SiF₄ / NH₃ mixtures](#)

J. Vac. Sci. Technol. A **22**, 570 (2004); 10.1116/1.1699335

[A comparative study on inductively-coupled plasma high-density plasma, plasma-enhanced, and low pressure chemical vapor deposition silicon nitride films](#)

J. Vac. Sci. Technol. A **18**, 372 (2000); 10.1116/1.582195

[Low dielectric constant films prepared by plasma-enhanced chemical vapor deposition from tetramethylsilane](#)

J. Appl. Phys. **85**, 3314 (1999); 10.1063/1.369677

[Infrared study of Si-rich silicon oxide films deposited by plasma-enhanced chemical vapor deposition](#)

J. Vac. Sci. Technol. A **15**, 377 (1997); 10.1116/1.580495

High-Voltage Amplifiers

- Voltage Range from $\pm 50V$ to $\pm 60kV$
- Current to 25A

Electrostatic Voltmeters

- Contacting & Non-contacting
- Sensitive to 1mV
- Measure to 20kV



ENABLING RESEARCH AND INNOVATION IN DIELECTRICS, ELECTROSTATICS, MATERIALS, PLASMAS AND PIEZOS



www.trekinc.com

TREK, INC. 190 Walnut Street, Lockport, NY 14094 USA • Toll Free in USA 1-800-FOR-TREK • (t):716-438-7555 • (f):716-201-1804 • sales@trekinc.com

Excitation mechanism and thermal emission quenching of Tb ions in silicon rich silicon oxide thin films grown by plasma-enhanced chemical vapour deposition—Do we need silicon nanoclusters?

A. Podhorodecki,^{1,(a)} L. W. Golacki,¹ G. Zatoryb,¹ J. Misiewicz,¹ J. Wang,² W. Jadwisienczak,² K. Fedus,³ J. Wojcik,⁴ P. R. J. Wilson,⁴ and P. Mascher⁴

¹*Institute of Physics, Wrocław University of Technology, Wybrzeże Wyspińskiego 27, 50-370 Wrocław, Poland*

²*School of EECS, Ohio University, Stocker Center 363, Athens, Ohio 45701, USA*

³*Institute of Physics, Nicholas Copernicus University, Grudziadzka 5/7, 87-100 Torun, Poland*

⁴*Department of Engineering Physics and Centre for Emerging Device Technologies, McMaster University, 1280 Main St. W, Hamilton, Ontario L8S4L7, Canada*

(Received 16 December 2013; accepted 31 March 2014; published online 10 April 2014)

In this work, we will discuss the excitation and emission properties of Tb ions in a Silicon Rich Silicon Oxide (SRSO) matrix obtained at different technological conditions. By means of electron cyclotron resonance plasma-enhanced chemical vapour deposition, undoped and doped SRSO films have been obtained with different Si content (33, 35, 39, 50 at. %) and were annealed at different temperatures (600, 900, 1100 °C). The samples were characterized optically and structurally using photoluminescence (PL), PL excitation, time resolved PL, absorption, cathodoluminescence, temperature dependent PL, Rutherford backscattering spectrometry, Fourier transform infrared spectroscopy and positron annihilation lifetime spectroscopy. Based on the obtained results, we discuss how the matrix modifications influence excitation and emission properties of Tb ions. © 2014 AIP Publishing LLC. [<http://dx.doi.org/10.1063/1.4871015>]

INTRODUCTION

Materials with potential use in CMOS technology have been extensively investigated in the past few decades. Potential applications based on those materials would lead to easy integration with various microelectronic devices. Because of its interesting optical properties, silicon rich silicon oxide (SRSO) has also been investigated for those purposes.^{1–6} The main advantage of SRSO is the presence of silicon nanoclusters (Si-NCs), which are optical centers and can serve as efficient sensitizers for lanthanide ions co-doped into the SRSO matrix. Additionally, introducing Si-NCs to SRSO improves the electrical properties of the oxide.⁷ Because of intense work over the past few years, practical devices such as red light emitting diodes (LEDs),⁸ memory devices,⁹ or photo-voltaic cells¹⁰ have been realized. Moreover, LEDs emitting in the infrared spectral range have also been already achieved based on Er³⁺ emission.^{7,11,12} Furthermore, promising results have also been obtained for SRSO doped with Nd³⁺ ions with strong emission at around 1100 nm.¹³ Recently, electroluminescence (EL) of Tb implanted silica thin films in MOS devices with external quantum efficiency as high as 10%^{14,15} and EL from a Tb-doped SiN matrix have also been shown.¹⁶

Thus, an interesting application of SRSO films, which so far has not been widely explored, is a green LED on a silicon substrate obtained in CMOS technology. This could be done by doping SRSO thin films with Tb³⁺ ions, which have a strong emission at 545 nm (2.27 eV). It has already been shown¹⁷ that the energy band gap (HOMO-LUMO) of

Si-NCs can be as wide as 2 eV for 3 nm nanocrystals and it can be increased over this value simply by forming smaller nanocrystals. Thus, theoretically, efficient excitation of Tb³⁺ ions via Si-NCs should be possible to achieve since their band gap can be wider than the required 2.27 eV.

In our recent paper,¹⁸ we have shown that emission from Tb³⁺ ions in an SRSO matrix can be observed at UV excitation and its intensity strongly depends on the Si concentration and annealing temperature. Surprisingly, it has been shown that only samples close to stoichiometric SiO₂ (35 at. % of Si) exhibit strong green emission, while the presence of Si-NCs, does not seem to be important in improving Tb³⁺ emission. Moreover, for those strongly emitting samples, the formation of clusters containing Tb ions has been confirmed at the film interface. Thermodynamic considerations suggest that the oxidized form of these clusters is favored.

The aim of this work is to understand the excitation mechanism of Tb³⁺ ions in SRSO films and how this mechanism depends on the Si concentration and the post-growth annealing temperature. There are a few possibilities of Tb³⁺ ion excitation in a SRSO matrix: (a) excitation through the charge transfer state (CTS),¹⁹ (b) via silicon nanoclusters,^{20,21} (c) defect states, or (d) via direct *f-d*²² or *f-f* transition²³ of Tb³⁺ ions. To investigate this aspect, the optical properties of the samples were investigated by means of photoluminescence (PL), PL excitation spectroscopy (PLE), time-resolved photoluminescence (TR-PL), absorption measurement, temperature dependent PL, and cathodoluminescence (CL). Structural data were obtained by means of Rutherford backscattering spectrometry (RBS), Fourier transform infrared spectroscopy (FTIR), and positron annihilation lifetime spectroscopy (PALS).

^{a)}E-mail: artur.p.podhorodecki@pwr.wroc.pl

To understand how the technological parameters influence the excitation mechanism of Tb^{3+} ions, we examined sets of SRSO and SRSO:Tb $^{3+}$ thin film samples grown by electron cyclotron resonance plasma-enhanced chemical vapour deposition (ECR-PECVD) with different Si concentrations and annealed at different temperatures (T_a) (see Table I for details).

EXPERIMENTAL DETAILS

Sample preparation

Tb doped SRSO thin films were grown on $\langle 100 \rangle$ Si substrates by ECR-PECVD. The silicon and oxygen precursors were silane (30% SiH_4 in Ar) and O_2 (10% O_2 in Ar), respectively. The oxygen flow rate was varied between 4 and 25 sccm in order to obtain samples with varying Si concentrations. Additional Ar gas was added to the plasma region in order to maintain the same deposition pressure of 2.1 mTorr for the undoped samples and 2.5 mTorr for Tb-doped samples, respectively. The β -diketonate organic compound tris (2,2,6,6-tetramethyl-3,5-heptanedionato)-Tb(III) ($\text{Tb}(\text{tmhd})^3$) was used as the Tb precursor. The Tb diffusion cell was heated up to 120 °C within a manifold to sublime the precursor and introduce it into the chamber alongside the silane, using Ar as the carrier gas. The Ar carrier gas flow was set constant at 5 sccm. During the deposition process, the substrate stage was heated to a temperature of 350 °C resulting in a sample surface temperature of 120 °C. Substrate rotation of 20 rpm was used to achieve uniformity and homogeneity of the grown films with average thickness of 200 nm. In the post-deposition process, the samples were cleaved into smaller pieces and annealed at temperatures from 600 to 1200 °C in a quartz tube furnace under flowing N_2 . Further details of the deposition system, film growth conditions, and films structure have been discussed previously.^{24,25}

EXPERIMENTAL TECHNIQUES

The FTIR spectra were collected using a Nicolet iS10 spectrometer (*Thermo Fisher Scientific Instruments, PA, USA*). These measurements were conducted in attenuated total reflectance mode (ATR) using a VariGATR accessory (*Harrick Scientific Products Inc, NY, USA*). Absorption spectra were collected with a JASCO V-570 spectrophotometer. The room-temperature PLE of the Tb^{3+} ions in the visible spectrum (VIS) was measured using an HR4000 spectrometer (*Ocean Optics, Dunedin, FL, USA*). As an excitation source, a 450 W Xe arc lamp connected to a Triax 180 monochromator (*Jobin-Yvon, Kyoto, Japan*) was used. The signal obtained was corrected to account for the spectral

TABLE I. Sets of samples with their specified parameters marked with # for SRSO samples and * for SRSO:Tb.

T_a	33 at. % Si	35 at. % Si	39 at. % Si	50 at. % Si
As deposited		#, *		
600 °C		#, *		
900 °C		#, *		
1100 °C	#, *	#, *	#, *	#, *

characteristic of the excitation source. PL as a function of temperature was excited using a 266 nm (*Elforlight, Daventry, UK*) pulsed laser with average power not exceeding 1 mW. An HR4000 spectrometer was used as the detection system for the measurements in the VIS. The PL decay was measured using a pulsed 266 nm laser coupled to a gated detection system (*QuantaMaster, Photon Technology International, London, Canada*).

The cathodoluminescence characterization was conducted using an electron beam of 10 keV and 1 mA/cm 2 (*STAIB Instrumente, Model EK-2035-R*). Samples were mounted on the cold finger of a closed-cycled helium refrigerator operating between 9 and 330 K. The CL spectra were dispersed by a 0.3 m spectrograph (*Acton Research, SpectraPro 300i*) and analyzed using a PI-MAX CCD camera (*Princeton Instrument*) equipped with a UV intensifier, operating in the spectral region from 200–950 nm.

PALS was used to investigate defects in the SRSO:Tb $^{3+}$ samples. The experiments were carried out using a fast-fast coincidence ORTEC PLS system equipped with plastic scintillators (*St. Gobain BC418*) and RCA 8850 photomultipliers.²³ The time resolution of the system was 180 ps in full width at half maximum (FWHM). The positron source $^{22}\text{NaCl}$ (10 μCi) in a 7 μm thick Kapton foil was sandwiched between two identical samples. The dynamic of each measurement was at least six orders of magnitude.

Film compositions were determined through RBS experiments conducted in the Tandetron Accelerator Laboratory at Western University in London, Canada using 1.0 MeV $^4\text{He}^+$ ions with an incident angle θ of 3° and random rotation of Φ to minimize substrate channeling. The atomic concentrations of elements (excluding hydrogen) as a function of depth in the film were calculated by fitting the RBS data using the QUARK simulation package after calibrating the experimental parameters against a reference sample consisting of a known dose of bismuth implanted into a silicon wafer.²⁶

EXPERIMENTAL RESULTS

In order to explore the evolution of structural properties of the SRSO matrix, we conducted FTIR measurements in the ATR mode for all samples. Figures 1(a) and 1(d) show FTIR spectra measured for SRSO:Tb $^{3+}$ samples as a function of annealing temperature and Si concentration. Additionally, a reference signal obtained for a high quality quartz film has been included in both graphs. It can be seen from each panel that the FTIR spectra have two main absorption bands in the spectral range from 700 to 1300 cm^{-1} . One is related to the Si-O-Si bending mode (band between 760 and 850 cm^{-1}) and the second one is attributed to the Si-O-Si stretching mode (band between 950 and 1100 cm^{-1}).²⁷ Figure 1 shows that with increasing Si concentration and reduction in annealing temperature, the position and broadening of these two peaks is changing. In both cases, the observed results can be related to the lowering of the degree of structural order of the SRSO matrix.²⁸

Figures 1(b) and 1(d) present quantitative analysis of FTIR spectra together with information on defect formation in the SRSO matrix supported by the PALS data (Figs. 1(b)

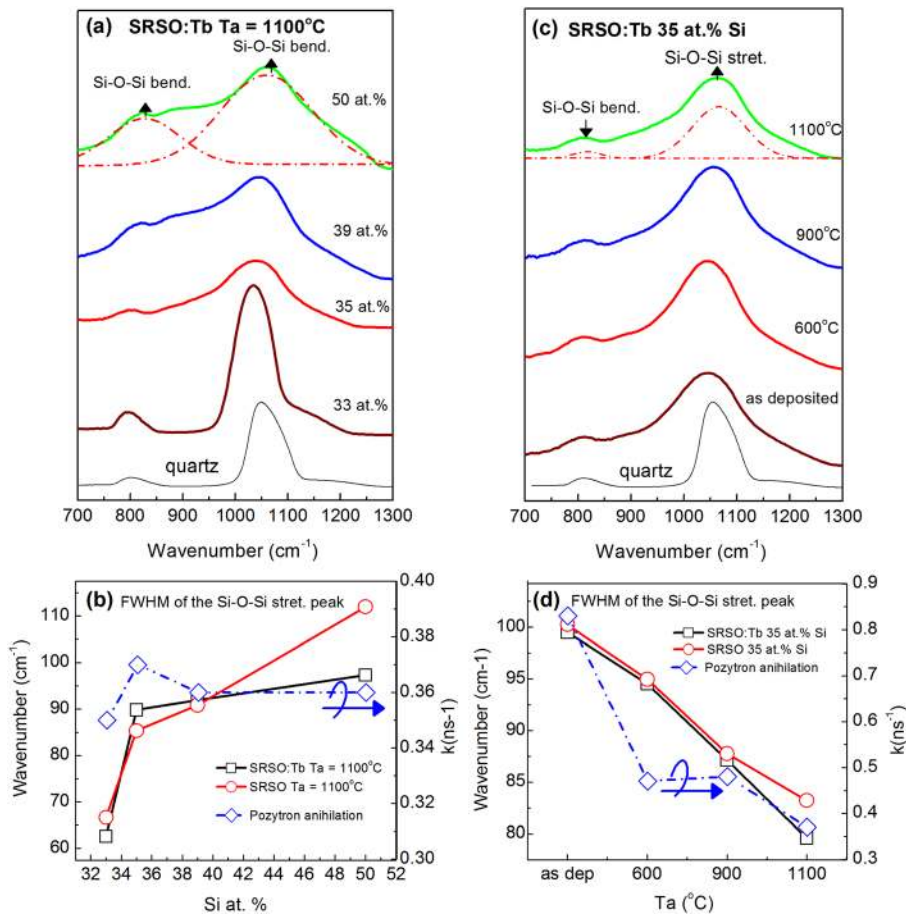


FIG. 1. FTIR spectra measured in ATR mode for (a) SRSO:Tb³⁺ films annealed at 1100 °C with different Si content and (c) SRSO:Tb³⁺ film with 35 at. % of Si annealed at different temperatures. FTIR peaks broadening (left scales) and positrons trapping rate (k^{-1}) rate from PALS experiment (right scales) obtained for (b) SRSO:Tb³⁺ with constant Si content and annealed at different temperatures and (d) SRSO:Tb³⁺ film with 35 at. % of Si annealed at different temperatures. Dashed lines in Figs. 1(a) and 1(c) show the Gaussians components of the fitting procedure used to analyze FTIR data.

and 1(d)). Figures 1(b) and 1(d) show the FWHM of the main FTIR peak as a function of Si concentration and the annealing temperature. The observed peak broadening can be attributed to the structural quality of the SRSO matrix. It can be seen from the figure that changes in Si concentration or annealing temperature significantly modified structural properties of the matrix. In the case of varying Si content, the matrix order became reduced with Si content increase from 33 at. % to 35 at. % while further increase in Si content has no significant effect on the matrix. Also, Fig. 1(d) clearly shows that increasing annealing temperature improves the structural quality of the films since the FWHM of the FTIR bands is significantly reduced.

This tendency towards matrix degradation with combined Si content increase and annealing temperature reduction corresponds to an increasing number of structural defects created in the SRSO matrix. The obtained FTIR results correlate well with the PALS results expressed by the positron trapping rate (k^{-1}) shown in Fig. 1(d) (right scale). It is known that positrons implanted in condensed matter can be trapped by neutral or negatively charged defects or in open spaces (voids or vacancies) before they annihilate with electrons.²⁹ The combination of these two trapping mechanisms could be responsible for the change of positron trapping rate in SRSO samples. These effects should be related mainly with annealing since this can be attributed to ordering (crystallization, densification) processes occurring in amorphous SiO₂ when heated at high temperature, as already observed using the positron Doppler-broadening technique.³⁰

The second possible positron annihilation route in SRSO could be related to Si precipitation and the formation of defect sites located at the Si/SiO₂ interfaces such as voids, E' centers ($\equiv \text{Si}^\bullet$, where the " \equiv " symbol stands for Si bonding with three O atoms), P_b centers ($\text{Si}_3 \equiv \text{Si}^\bullet$), peroxy radicals ($\equiv \text{Si} - \text{O} - \text{O}^\bullet$), and non-bridging O hole centers (NBOHC) ($\equiv \text{Si} - \text{O}^\bullet$).^{31,32} Nevertheless, in order to get a detailed picture of the nature of positron trapping states, more precise depth-resolved positron annihilation measurements (using variable energy positron beam) must be performed. The absence of a dependence of k^{-1} rate on the Si concentration does not exclude the creation of new defects, but suggests that these defects are not sensitive to the PALS technique.

Analyzing PALS on SRSO:Tb³⁺ samples (\square) and FTIR on SRSO samples (\circ) data shown in Figs. 1(b) and 1(d), we have not found any evidence that the Tb³⁺ ion doping affects the evolution of structural properties of the SRSO matrix within the studied Si concentrations and annealing temperatures.

Figure 2 shows total photoluminescence excitation (TPLE), cw-PL ($\lambda_{\text{EXC}} = 266$ nm), and absorption spectra obtained for selected samples. Figure 2(a) shows a strong emission from the SRSO matrix at 550 nm. We attributed this emission to the radiative recombination of defect states in the SRSO matrix or from very small amorphous nanoclusters²¹ because Raman spectroscopy studies¹⁸ have indicated that Si-NCs were not present at this Si concentration. Typically, one may expect to find a few potential defect states (e.g., NBOHC, oxygen deficient center (ODC), or the

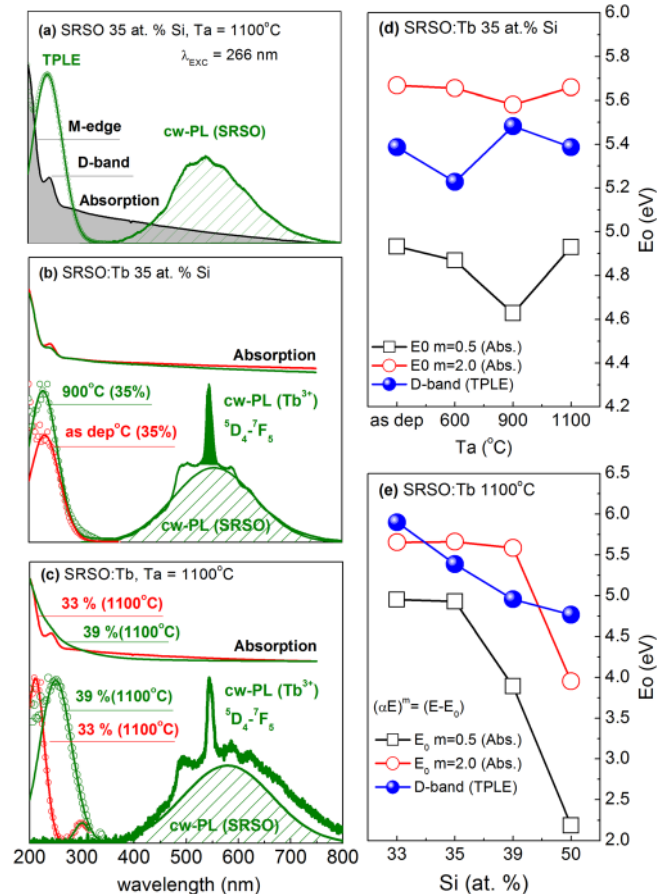


FIG. 2. TPLe, PL ($\lambda_{\text{exc}}=266$ nm), and absorption spectra obtained for (a) SRSO sample with 35 at. % Si annealed at 1100 °C, (b) SRSO:Tb³⁺ samples with 35 at. % Si annealed at 900 °C (green line) and as deposited (red line), (c) SRSO:Tb³⁺ sample with 39 at. % Si and 33 at. % Si annealed at 1100 °C. Values of absorption edge (M-edge) and TPLe peak position (D-band) obtained for SRSO:Tb³⁺ samples (d) with 35 at. % Si and annealed at different temperatures, (e) containing different Si at. % and annealed at 1100 °C.

self-trapped exciton (STE)) in silica based materials such as SRSO. It is expected that by measuring TPLe spectra, we can obtain insight into the nature on these defects. The TPLe spectrum measured for undoped SRSO (Fig. 2(a)) exhibits an absorption edge above 200 nm (6.19 eV, M-edge) and a strong excitation band at 240 nm (5.1 eV, D-band). The energies of these two bands are in good agreement with the absorption band energies also shown in Fig. 2(a). It is known that NBOHCs have an absorption band at 4.8 eV and 5.8 eV in wet SiO₂ films,³³ but it has been shown that it can be present in both wet and in dry silica.³⁴ Thus, NBOHCs exist with E' center defect states which typically have absorption bands from 5.3 eV to 6.2 eV.³⁵ Considering that the position of NBOHC bands can shift in different materials, this can be a good candidate for the radiative defects (RD) responsible for the observed emission from the SRSO matrix. However, the ODC is another type of defect which has very similar shape compare to the D-band and one of the main absorption bands at ~ 5.1 eV.³⁶ This defect center is a neutral oxygen vacancy and is indicated generally as $\equiv\text{Si}-\text{Si}\equiv$.³⁷ In addition, several models have been proposed in the literature attempting to clarify the STE defect states^{38,39} with a band also at ~ 5.2

eV.⁴⁰ They are based on the idea that the silicon-oxygen bond (Si-O) gets ruptured and forms an oxygen-oxygen bond (-O-O-).⁴⁰ Thus, justifications on the nature of the defects responsible for the observed emission are not possible based solely on the optical data.

Figure 2(b) shows PL, TPLe, and absorption spectra obtained from Tb-doped SRSO samples (~ 1 at. % Tb) as deposited and annealed at 900 °C. The Tb-doped SRSO exhibits a superposition of a strong and broad emission band at 550 nm related to the SRSO matrix and the sharp and strong $f-f$ emission lines of Tb³⁺ ions. To overcome the problem of superposition of overlapping signals at a specific energy, TPLe⁴¹ has been measured, where only the intensity of Tb³⁺ related emission has been analyzed as a function of the excitation wavelength. The obtained TPLe spectrum has the same shape as the one obtained from the reference SRSO matrix. Two bands can be clearly resolved in this case, one at 240 nm and a second below 200 nm. This indicates that the excitation mechanism of optically active Tb³⁺ ions is the same to the one resulting in SRSO matrix related emission. If this is true, this result indicates efficient coupling between defects states and Tb³⁺ ions and energy transfer between these two objects. Moreover, we can see from Fig. 2(b) that post growth annealing of SRSO:Tb³⁺ films does not significantly influence the absorption nor the TPLe spectra. To analyze the influence of Si concentration on the excitation mechanism of Tb³⁺ ions, the same set of experiments was conducted for samples with 39 and 33 at. % of Si annealed at 1100 °C. The results are shown in Fig. 2(c). It can be seen that the PL spectrum does not change significantly upon increasing the Si concentration. However, the maximum of the TPLe spectrum is shifted significantly (~ 1.5 eV) towards lower energies when the Si content changed from 33 to 50 at. % (see Fig. 2(e)). Considering quantum confinement effects, the Si concentration dependent peak position suggests that Tb³⁺ ions can be excited via Si-NCs.²¹ Two arguments, however, are against this explanation. First, for small Si content, we did not find nanocrystals inside the matrix with Raman spectroscopy. Second, the obtained band position is far above the values expected for Si nanocrystals. Recently, Gresback *et al.*¹⁷ reported values for E' transitions of 3.6 eV for 3.9 nm Si nanocrystals. Keeping in mind that these higher energy levels only slightly depend on the nanocrystal size, even this value is much lower than the one that we have obtained. Thus, the most suitable explanation is that the Si concentration influences the formation of defects. It seems, however, that these optically active defects (Si content dependent) are different than the defects which are sensitive to position trapping (not dependent on Si content, annealing dependent). Thus, an increase in the number of defects in the SRSO matrix could change the broadening of the density of states tail of the matrix resulting in a shifting of the excitation profile obtained for both the SRSO matrix and the Tb³⁺ ion emission towards lower energies.

The absorption spectrum of SRSO also changes significantly with Si content and the D-band observed for samples with lower Si concentrations became unresolved at higher Si concentrations. Much less variation in the position of the absorption and excitation bands (small shift of the M-edge

towards lower energies) has been observed for samples annealed at different temperatures as seen in Fig. 2(d). Analyzing the data shown in Figs. 2(d) and 2(e), one can conclude that annealing only slightly influences the absorption edge (M-edge) of the matrix and the excitation mechanism of Tb^{3+} ion in contrast to the Si concentration effect. Similar conclusions have already been reported for undoped SRSO films.¹

Results presented so far show that Tb^{3+} ions are excited via energy transfer from defect states formed in the SRSO matrix rather than Si-NCs. Moreover, these defect states (D-band), which seem to be related to deep defects, allow efficient localization of electron-hole pairs and efficient energy transfer to Tb^{3+} ions via the strongly allowed $f-d$ transition. This is because of D-band overlaps with the predicted energy range for efficient $f-d$ transitions in Tb ions. The position of this band varies from sample to sample, but is usually located in the range between 200–300 nm, i.e., at 270 nm for the YAIO_3 matrix.²²

Frequently, optimization of the parameters of the lanthanide-doped solid state matrices for LEDs using PL results is misleading. This is because the excitation mechanism of lanthanides with photons (optical pumping) and electrons (impact excitation and ionization) can be very different. As a consequence, samples with strong PL can exhibit weak electroluminescence and vice versa. To analyze this aspect, the light generation for the studied samples was examined for three different types of excitation regimes.

Figure 3 shows room temperature emission spectra obtained for a SRSO: Tb^{3+} sample with 35 at. % of Si annealed at 1100 °C under *cw*-PL, TR-PL, and *cw*-CL excitations, respectively. Comparing the spectra shown in Figs. 3(a) and 3(b), one can see that the SRSO matrix related emission disappeared when the signal was collected with a delay of 10 μs after the 266 nm excitation pulse. This indicates that the luminescence kinetics of this matrix-related band are much faster than the Tb^{3+} ion luminescence decay time.

Recently, we have reported on similar effects in SRSO: Er^{3+} films, where the decay times of the matrix-related emission band were estimated as close to 20 ns.²¹ Figure 3(c) shows the CL spectrum measured with constant (*cw*) energetic electron current bombarding the sample surface. It is seen that the CL spectrum is similar to the *cw*-PL spectrum; however, the broad SRSO matrix related emission intensity is significantly quenched. The two excitation techniques (PL vs. CL) giving rise to the luminescence of Tb^{3+} ions have some common features and a difference in excitation processes. In PL, each photon that is absorbed with an energy higher than the absorption edge produces a single electron-hole ($e-h$) pair. In the case of CL, all excitation processes are simultaneously present in contrast to the PL (e.g., at 266 nm), when only specific excitation/energy transfer processes are allowed. The electron acceleration energy of a few keV (10 keV for the CL study) is sufficient for generating multiple $e-h$ pairs in the SRSO matrix, Si nanoclusters, or defects despite their large band gaps (9–11 eV for SiO_2 and ~ 3.5 –1.5 eV for Si nanoclusters). Energetic electrons interacting with a solid state host lose kinetic energy primarily through inelastic valence-electron

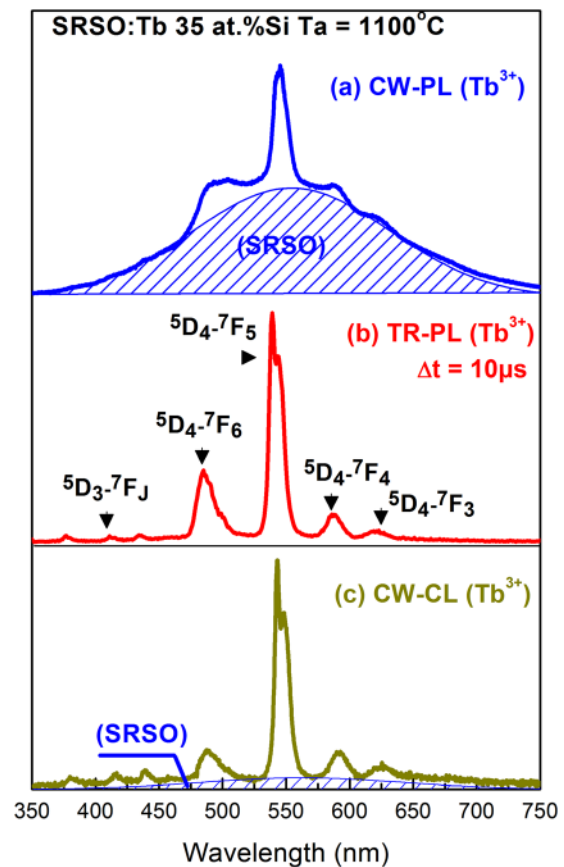


FIG. 3. Spectra of SRSO: Tb^{3+} with 35 at. % Si annealed at 1100 °C generated by various excitations (a) *cw*-PL ($\lambda_{\text{EXC}} = 266$ nm), (b) TR-PL ($\lambda_{\text{EXC}} = 266$ nm), and (c) *cw*-CL. Segments (a) and (c) show the broad emission band of the SRSO matrix extracted from *cw*-PL (a) and *cw*-CL (c) spectra.

scattering events creating hot electrons and holes.⁴² Hot carriers thermalize within a few picoseconds to states near the conduction and valence band edges where they diffuse before recombining by radiative or nonradiative processes. This is especially true for large band gap systems. Some carriers can also be trapped by surface or point defects. Due to specific selection rules, the excitation of Tb^{3+} ions via the creation of $e-h$ pairs during CL is more restricted than impact excitation by energetic electrons, which is governed primarily by momentum and energy conservation principles. However, both processes can benefit multiple times from a single energetic electron contributing to the Tb^{3+} ion excitation process during cascading kinetic energy reduction.

In the case of the PL of Tb^{3+} ions stimulated by indirect optical excitation, the energy of $e-h$ pairs localized at defect states is nonradiatively transferred to the Tb^{3+} ion $4f^n$ electron system. Generally, the excitation by energetic electrons produces emission via all possible luminescence mechanisms available. However, in the case of the SRSO: Tb^{3+} matrix, the direct impact excitation and excitation via ionization of other impurities are more effective in exciting optically active Tb^{3+} ions than energy transfer from recombining $e-h$ pairs. As a consequence, the final ratio of Tb^{3+} ion-related emission intensity to matrix related emission intensity is much higher in the case of CL (factor of 1/1) than in PL (factor of 1/18).

Figure 4(a) shows the integrated emission intensities of Tb^{3+} ions obtained from *cw*-PL, TR-PL, and *cw*-CL experiments, plotted as a function of annealing temperature for SRSO: Tb^{3+} samples with 35 at. % Si (Figs. 4(a) and 4(b)) and for SRSO: Tb^{3+} samples with varied Si concentration which were annealed at 1100 °C (Fig. 4(c)). The presented values are normalized with respect to the PL intensity of the as-deposited SRSO: Tb^{3+} sample. It can be seen that the Tb^{3+} ion emission intensity observed in all three experiments increased with the annealing temperature. However, the CL emission intensity increases faster than in the case of optical excitations due to the differences in Tb^{3+} ion excitation processes involved as discussed above.

The emission intensity increase in response to an increase in the annealing temperature can be related to (a) reduction in the number of nonradiative channels (nonradiative defects, NRD) coupled with Tb^{3+} ions, (b) crystallization of the matrix (local crystal field modification), (c) increase in the refractive index of the matrix, or (d) increase in the number of sensitizer (radiative defects, RD) responsible for the Tb^{3+} ions' excitation, or (e) better coupling between them.

The PALS and FTIR results have shown that the number of defects (NRD and/or RD) is reduced after thermal annealing treatment. On the other hand, absorption and TPLE show that the number of optically active defects (RD) is not changing during the annealing. Thus, the observed results most probably are related to a reduction of nonradiative centers (NRD) in the matrix as detected by PALS.

Careful analysis of the results shown in Fig. 4(b) revealed that the intensity of the Tb emission band and the SRSO matrix emission both increase in a similar manner with increasing annealing temperature. The plausible explanation of this effect is that these optically active defects (RD) are coupled with other NRDs similar to the Tb ions. Thus, reduction of nonradiative defects with annealing (PALS) increases the emission from both Tb ions and radiative defects in the SRSO matrix. Moreover, we can assume tentatively that the main loss of carriers is not at the Tb^{3+} ion induced energy level but rather for carriers which are localized at intermediate defect states participating in Tb^{3+} ion excitation.

Furthermore, assuming that these intermediate optically active defects are coupled with Tb^{3+} ions, anti-correlation

behavior of radiative emission intensities from the matrix and $4f$ -shell transitions would be expected. This is not the case. Thus, the broad emission band centered at 550 nm observed in SRSO: Tb^{3+} samples is defect related but these defects are not coupled effectively to the Tb^{3+} ions. Under these circumstances, the considered emission bands originate separately from the RD-NRD and RD-NRD- Tb^{3+} complexes, respectively, where the energy from the RD (D-band) in the RD-NRD- Tb^{3+} complex is transferred more effectively to the Tb^{3+} ion $4f$ -shell system as compared with the isolated defect RD-NRD from which the energy is mainly emitted radiatively. These processes have been schematically presented in Fig. 4(b). Based on these assumptions, annealing reduces the number of NRDs, thereby simultaneously increasing the intensity of emission from both the Tb^{3+} ions and the radiative defects formed inside the SRSO matrix.

Figure 4(c) shows the change in Tb^{3+} ion emission intensity in SRSO: Tb^{3+} samples as a function of different Si concentrations. It is clearly seen that the Tb^{3+} ion emission intensity resulting from different excitations is reduced significantly when the Si content is changed from 35 to 50 at. %. Moreover, in this case, the Tb^{3+} ion emission intensity reduction is more significant (factor of 16) as compared to the annealing effect (factor of 2). We correlate this observation with the possibility of the creation of additional nonradiative centers (NRD) in the SRSO matrix or changes in the local Tb environment. Relying on the discussion presented in Ref. 18, we can expect that the higher Si content in the studied SRSO: Tb^{3+} samples contributed to effective dissociation of the TbO clusters, which resulted in a more homogeneous distribution of Tb^{3+} ions throughout the SRSO matrix but with much lower emission. As a consequence, one can speculate that excitation of a Tb^{3+} ion in a TbO cluster is more efficient than an isolated Tb^{3+} ion coupled either to defects or Si nanoclusters in the SRSO matrix. It recently has been shown by us using Raman spectroscopy¹⁸ that a reduction in Tb^{3+} ion emission intensity can be correlated with the formation of Si-NCs in the SRSO matrix. Thus, we believe that Si-NCs are ineffective sensitizers of Tb^{3+} ions as emitting centers in the SRSO matrix. They can even serve as accumulation centers for Tb ions, enhancing Tb clustering and consequently quenching their emission.

Thus, to obtain the most efficient emission from Tb^{3+} ions in the SRSO matrix, we should increase the number of

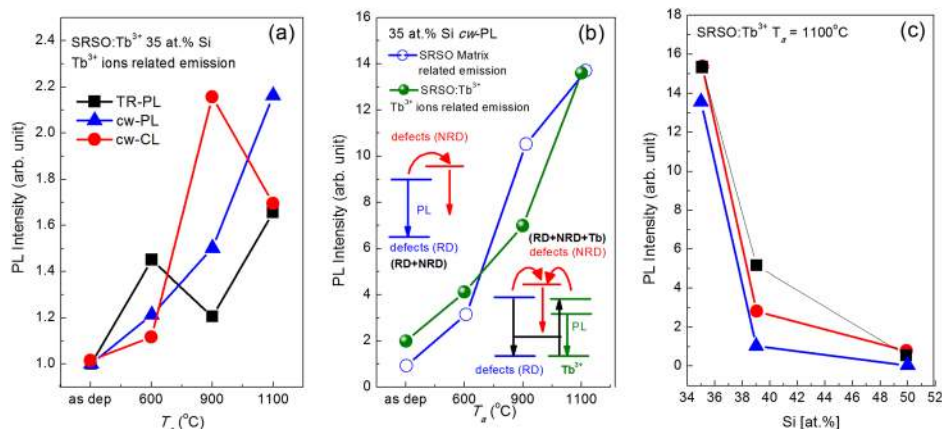


FIG. 4. (a) Total emission intensity for SRSO: Tb^{3+} samples under different excitations, (b) *cw*-PL emission intensity for the undoped SRSO matrix and Tb^{3+} ions present in the SRSO: Tb^{3+} host, (c) dependence of *cw*-PL intensity for SRSO: Tb^{3+} vs. Si concentration. TR-PL—time resolved photoluminescence intensity, *cw*-PL—continuous excitation/detection photoluminescence intensity, *cw*-CL—continuous excitation/detection cathodoluminescence intensity.

Tb³⁺ ions coupled to optically active defects (i.e., increase of Tb³⁺ concentration) and, at the same time, reduce the number of non-radiative defects in the matrix (low Si content, high annealing temperature).

THERMAL QUENCHING

It is known that materials in which ions are excited from defect states through the *f-d* transitions exhibit strong thermal quenching due to the fact that *5d* electrons are delocalized and interact readily with the local environment (defects via phonons). Thus, it is expected that thermal quenching should increase with Si content and be reduced with higher annealing temperature.

Figure 5 shows the thermal quenching data of the Tb³⁺ ion and SRSO matrix related emission intensity obtained for SRSO:Tb³⁺ samples with 35 at. % Si (Figs. 5(a)–5(c)) and 39 at. % Si (Figs. 5(d)–5(f)), respectively, as a function of annealing temperature. Experimental results in Fig. 5 have been fitted with the double Arrhenius equation (1)

$$I(T) = \frac{I_0}{1 + A_1 \exp\left(-\frac{E_1}{kT}\right) + A_2 \exp\left(-\frac{E_2}{kT}\right)}, \quad (1)$$

where $k = 8.62 \times 10^{-5}$ [eV/K] (Boltzmann constant) and E_1 , E_2 are thermal quenching energies. It is worth mentioning, however, that due to the complexity of the analyzed signal

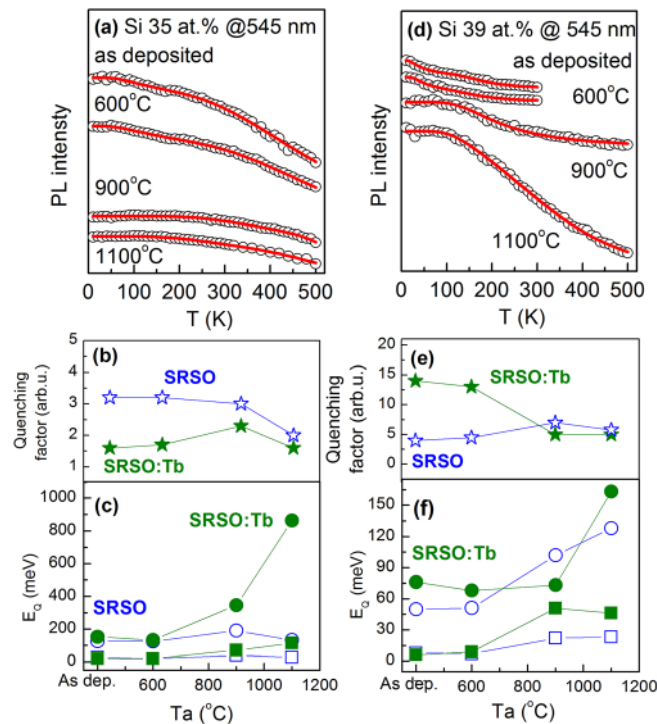


FIG. 5. Emission intensity of Tb³⁺ ions vs. temperature together with fitting curves for SRSO:Tb samples annealed at different temperatures and with different Si content (a) 35 at. % and (d) 39 at. %. Quenching factors of emission obtained for Tb emission (full stars) and SRSO emission (empty stars) for samples with (b) 35 Si at. % and (e) 39 Si at. %. Thermal quenching energies obtained for Tb emission (full circles and squares) and SRSO emission (empty circles and squares) for samples with (c) 35 Si at. % and (f) 39 Si at. %.

and the weak signal intensity for certain samples, the obtained results should be analyzed more in a qualitative than a quantitative manner.

From Figs. 5(a)–5(c), it can be seen that for SRSO:Tb³⁺ samples with 35 at. % Si, the thermal quenching of Tb³⁺ ion and SRSO matrix related emission is weak (factor of 2) and is almost annealing temperature independent. This can be understood when considering the fact that estimated Tb³⁺ ion quenching energies (E_1) are relatively high (from 100 to 200 meV). E_1 increases up to 1 eV for the SRSO:Tb³⁺ sample annealed at 1100 °C. Such a high value of thermal quenching energy guarantees very good thermal stability of Tb³⁺ ion related emission intensity from the SRSO:Tb³⁺ samples with 35 at. % Si annealed at 1100 °C. We believe that the energy available for exciting optically active Tb³⁺ ions is partially lost before the transfer from SRSO matrix defects to the Tb³⁺ ions occurs. This is the dominating mechanism over the energy back transfer from the Tb³⁺ ions to the SRSO matrix due to the strong coupling of *5d* states with defects.

In contrast, SRSO:Tb³⁺ samples with 39 at. % Si behave differently. Figs. 5(d)–5(f) show that the thermal quenching of Tb³⁺ ions in these samples is more significant (factor of 15, Fig. 5(e)) and exhibits a strong dependence on annealing conditions. Annealing at higher temperatures reduced the magnitude of the thermal quenching of the Tb³⁺ ion by a factor of 5. The estimated thermal quenching energy for the SRSO:Tb³⁺ samples with 39 at. % Si annealed at 1100 °C is ~150 meV and is much smaller than for the SORS:Tb³⁺ sample with 35 at. % Si. Thus, the low thermal barrier between the *5d* levels of Tb and defect states make this quenching very efficient. The SRSO matrix emission does not show significant thermal quenching in the studied temperature range and is less dependent on post-growth annealing and Si content.

The analysis of thermal quenching processes involved in the luminescence of samples excited by energetic electrons (*cw*-CL) is complicated due to the plethora of available energy relaxation channels. Figures 6(a) and 6(b) show CL spectra of SRSO:Tb³⁺ samples with 35 at. % Si annealed at different temperatures and recorded at 10 and 300 K, respectively. The CL spectra are dominated by the Tb³⁺ ion *4f-f* shell ⁵D₄-⁷F₅ transition line at 550 nm and are accompanied by less intense transition lines originating from ⁵D₃ and ⁵D₄ levels and terminating at ⁷F_J levels. It can be seen from Fig. 6 that the SRSO:Tb³⁺ sample annealed at 900 °C generates the strongest Tb³⁺ ion emission intensity at room temperature (see inset in Fig. 6(a)). As can be seen from the inset, the CL intensity has completely different behavior with temperature compared to the PL intensity. These results may indicate that the carrier's thermal diffusion processes are involved in the Tb³⁺ ion's excitation process at elevated temperatures along with the typical CL relaxation mechanisms.

Figures 7(a) and 7(b) show CL spectra of SRSO:Tb³⁺ samples with different Si content measured at 10 and 300 K. It is seen that the room temperature Tb³⁺ ion emission intensity in the sample with 33 at. % of Si is a factor of 20 stronger than at low temperature. We can speculate that thermally

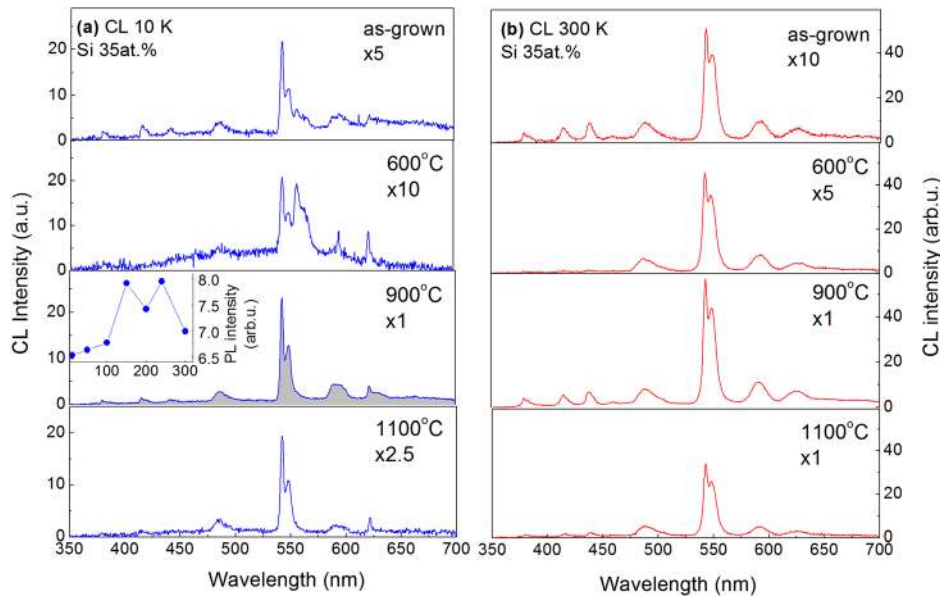


FIG. 6. Normalized (a) low temperature and (b) room temperature CL spectra of SRSO:Tb³⁺ samples with 35 at. % of Si annealed at different temperatures. The inset in (a) shows the temperature dependent integrated global Tb³⁺ ion emission intensity for a sample annealed at 900°C.

stimulated charge trapping/releasing processes and/or, however less probable, defect creation (e.g., vacancies) by energetic electrons can be considered to explain the observed CL intensity variation. This requires energetic electrons accelerated with energy typically greater than hundreds of keV. Furthermore, only a small fraction of the incident electron's kinetic energy can be transferred to host atoms in non-relativistic collisions, (i.e., ~ 0.36 eV for 2 keV electrons in the case of diamond), far below the energy transfer threshold required to create knock-on vacancies in typical solid state hosts.⁴³ Also, the local heating effect during CL excitation should be considered as well due to the low thermal conductivity of SiO₂ (~ 1 W/mK) and the relative large electron current density (~ 1 mA/cm²) employed. Specifically, electron beam heating can be considered by assuming that

energy is uniformly deposited in a sphere of a certain radius (~ 1 nm) for a given acceleration voltage (10 keV).⁴² Based on the currently available experimental results, we conclude that SRSO:Tb³⁺ samples subjected to electron excitation during CL with energy of 10 keV and current density of ~ 1 mA/cm² may stimulate partial removal of both structural and chemical disorder resulting in modification of the Tb³⁺ ions' local environment along with thermal charge trapping/releasing processes as discussed above. It is documented in the literature that thermally annealed amorphous semiconductors experience some structural reordering (not necessarily crystallization).^{44,45} It is believed that when this takes place, the dangling or broken bonds and/or the atomic rearrangements of the amorphous material may have great influence on the electronic states of amorphous host.

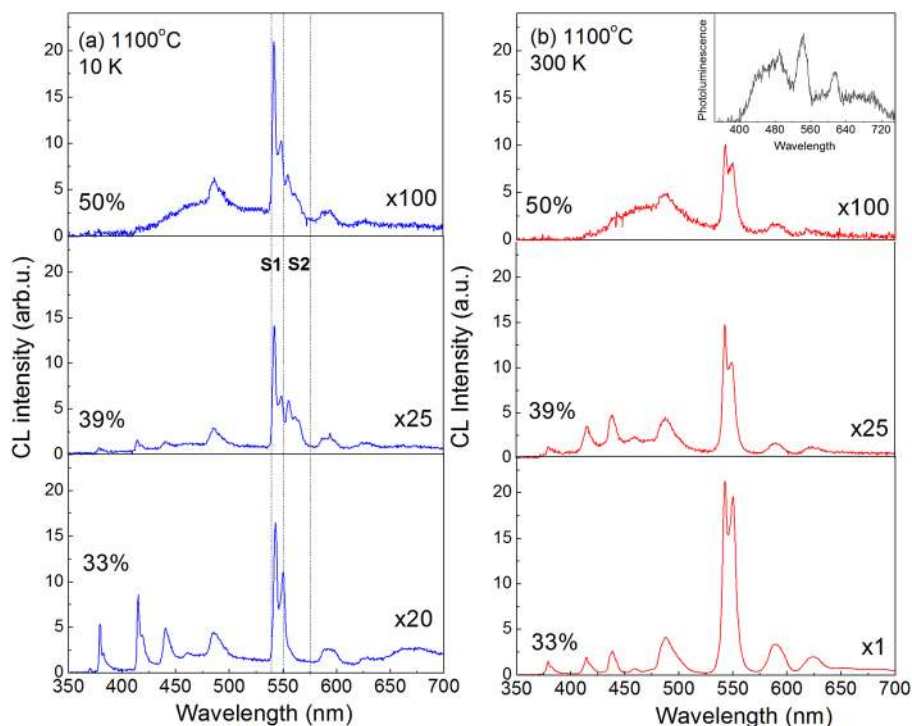


FIG. 7. CL spectra of SRSO:Tb³⁺ samples with different Si content annealed at 1100°C measured at (a) 10 K and (b) 300 K. CL spectra were measured with the same excitation (5 keV, ~ 70 μ A/cm²) and detection conditions. All CL spectra were normalized with respect to the strongest CL emission line observed. The inset shows the temperature dependence of integrated Tb³⁺ ion green emission intensity for a sample with 33 at. % of Si annealed at 1100°C.

Moreover, from Fig. 7, it is clear that for samples with higher Si concentration, an additional strong emission band centered at 450 nm appears. Appearance of this band for Si concentrations higher than 40 at. % correlates with the Raman spectra indicating the presence of Si nanoclusters in the SRSO matrix. In this case, however, we can see that the CL intensity from Tb ions introduced into SRSO matrix is lower by factor of 100 when compared to samples with no clear indication of Si nanoclusters formation. Finally, detailed analysis of CL spectra at 10 K shows a much more complicated Tb emission line shape for samples with higher Si concentration. The spectra suggest the existence of two significantly different sites for Tb ions. One site can be related to Tb ions coordinated in a more oxygen rich environment (i.e., Tb_xO_y clusters) while the second site can be attributed to Tb ions localized in a more silicon rich environment (i.e., at Si-NCs/SiO₂ interface).

CONCLUSIONS

In this work, it has been shown that SRSO:Tb films exhibit highly intense green emission when excited either with photons or electrons. We have shown that the presence of Si nanoclusters in SRSO films obtained with high Si at. % and annealed at high temperature does not correlate with a high emission intensity from Tb ions. Further, the obtained results suggest that for films containing Si nanoclusters, Tb emission is significantly reduced as compared to films with no indication of Si nanoclusters when excited either optically and with high energy electrons.

It has also been shown that in the case of optical excitation, only a small fraction of Tb ions are excited via the energy transfer from defect states in the matrix, while in the case of electronic excitation, many more Tb ions seem to be activated via other excitation channels (i.e., impact ionization). Also, a significant defect related emission from the matrix itself has been found for all investigated samples. It has been proposed that both types of emission (Tb and SRSO) originate from energy levels coupled to defects that serve as channels of nonradiative recombination.

ACKNOWLEDGMENTS

A.P. would like to acknowledge financial support from the Iuventus Plus Program (No. IP2011 042971). In Canada, the work was supported by the Natural Sciences and Engineering Research Council of Canada (NSERC) under the Discovery Grants Program. W.M.J. acknowledges the support from the NSF CAREER Award No. DMR-1056493.

¹A. Podhorodecki, G. Zatyrb, J. Misiewicz, J. Wojcik, and P. Mascher, *J. Appl. Phys.* **102**, 043104 (2007).

²X. J. Hao, A. Podhorodecki, Y. S. Shen, G. Zatyrb, J. Misiewicz, and M. A. Green, *Nanotechnology* **20**, 485703 (2009).

³F. Gourbilleau, X. Portier, C. Ternon, P. Voivenel, R. Madelon, and R. Rizk, *Appl. Phys. Lett.* **78**, 3058–3060 (2001).

⁴V. Vinciguerra, G. Franzò, F. Priolo, F. Iacona, and C. Spinella, *J. Appl. Phys.* **87**, 8165 (2000).

⁵C. Garcia, B. Garrido, P. Pellegrino, R. Ferre, J. A. Moreno, J. R. Morante, L. Pavesi, and M. Cazzanelli, *Appl. Phys. Lett.* **82**, 1595 (2003).

⁶N. Daldosso, M. Luppi, S. Ossicini, E. Degoli, R. Magri, G. Dalba, P. Fornasini, R. Grisenti, F. Rocca, L. Pavesi, S. Boninelli, F. Priolo, C. Spinella, and F. Iacona, *Phys. Rev. B* **68**, 085327 (2003).

⁷J. M. Ramírez, F. Ferrarese-Lupi, O. Jambois, Y. Berencén, D. Navarro-Urrios, A. Anopchenko, A. Marconi, N. Prtljaga, A. Tengattini, L. Pavesi, J. P. Colonna, J. M. Fedeli, and B. Garrido, *Nanotechnology* **23**, 125203 (2012).

⁸J. De La Torre, A. Souifi, A. Poncet, C. Busseret, M. Lemiti, G. Bremond, G. Guillot, O. Gonzalez, B. Garrido, J. R. Morante, and C. Bonafos, *Phys. E* **16**, 326 (2003).

⁹L. Khomenkova, X. Portier, B. Sahu, A. Slaoui, C. Bonafos, S. Schamm-Chardon, M. Carrada, and F. Gourbilleau, *ECS Trans.* **35**, 37 (2011).

¹⁰I. Perez-Wurfl, L. Ma, D. Lin, X. Hao, M. A. Green, and G. Conibeer, *Sol. Energy Mater. Sol. Cells* **100**, 65 (2012).

¹¹L. Tsybeskov, S. P. Duttagupta, K. D. Hirschman, P. M. Fauchet, K. L. Moore, and D. G. Hall, *Appl. Phys. Lett.* **70**, 1790 (1997).

¹²G. Z. Ran, Y. Chen, W. C. Qin, J. S. Fu, Z. C. Ma, W. H. Zong, H. Lu, J. Qin, and G. G. Qin, *J. Appl. Phys.* **90**, 5835 (2001).

¹³P. Pirasteh, J. Charrier, Y. Dumeige, J. L. Doualan, P. Camy, O. Debieu, Ch. Liang, L. Khomenkova, J. Lemaître, Y. G. Boucher, and F. Gourbilleau, *J. Appl. Phys.* **114**, 014906 (2013).

¹⁴J. M. Sun, W. Skorupa, T. Dekorsy, M. Helm, L. Rebohle, and T. Gebel, *J. Appl. Phys.* **97**, 123513 (2005).

¹⁵M. E. Castagna, S. Coffa, M. Monaco, A. Muscara, L. Caristia, S. Lorenti, and A. Messina, *Mater. Sci. Eng., B* **105**, 83 (2003).

¹⁶Y. Berencén, R. Wutzler, L. Rebohle, D. Hiller, J. M. Ramirez, J. A. Rodriguez, W. Skorupa, and B. Garrido, *Appl. Phys. Lett.* **103**, 111102 (2013).

¹⁷R. Gresback, Y. Murakami, Y. Ding, R. Yamada, K. Okazaki, and T. Nozaki, *Langmuir* **29**, 1802 (2013).

¹⁸A. Podhorodecki, G. Zatyrb, J. Misiewicz, J. Wojcik, P. R. J. Wilson, and P. Mascher, *Nanotechnology* **23**, 475707 (2012).

¹⁹P. Dorenbos, *J. Phys.: Condens. Matter* **15**, 8417 (2003).

²⁰E. Gross, D. Kovalev, N. Kunzner, J. Diener, F. Koch, V. Y. Timoshenko, and M. Fujii, *Phys. Rev. B* **68**, 115405 (2003).

²¹A. Podhorodecki, G. Zatyrb, L. W. Golacki, J. Misiewicz, J. Wojcik, and P. Mascher, *Nanoscale Res. Lett.* **8**, 98 (2013).

²²A. Podhorodecki, M. Banski, J. Misiewicz, J. Serafinczuk, and N. V. Gaponenko, *J. Electrochem. Soc.* **157**, H628 (2010).

²³B. M. Walsh, “Judd-Ofelt theory: Principles and practices,” in *Advances in Spectroscopy for Lasers and Sensing, Proceedings of the NATO Advanced Study Institute on New Developments in Optics and Related Fields, in Erice, Sicily, Italy, 6–21 June 2005*, NATO Science Series: Series II: Mathematics, Physics and Chemistry, Vol. 231, edited by B. Di Bartolo and O. Forte (Springer, 2006), pp 403–433.

²⁴M. Boudreau, M. Boumerzoug, P. Mascher and P. E. Jessop, *Appl. Phys. Lett.* **63**, 3014 (1993).

²⁵A. Karbowski, J. D. Fidelus, and G. P. Karwasz, *Mater. Sci. Forum* **666**, 155 (2010).

²⁶W. N. Lennard, The QUARK simulation package for RBS is available from the author at wlennard@uwo.ca, 2012.

²⁷H. Aguiar, J. Serra, P. González, and B. León, *J. Non-Cryst. Solids* **355**, 475 (2009).

²⁸G. Zatyrb, A. Podhorodecki, J. Misiewicz, J. Cardin, and F. Gourbilleau, *Nanoscale Res. Lett.* **8**, 40 (2013).

²⁹R. Krause-Rehberg and H. S. Leipner, *Positron Annihilation in Semiconductors, Defect Studies*, Springer Series in Solid-State Sciences 127 (Springer, Berlin, 1999).

³⁰G. Brauer and G. Boden, *Appl. Phys.* **16**, 119 (1978).

³¹G. Brauer, G. Boden, A. Balogh, and A. Andreeff, *Appl. Phys.* **16**, 231 (1978).

³²M. Fujinami and N. B. Chilton, *Appl. Phys. Lett.* **64**, 2806 (1994).

³³G. Pacchioni, L. Skuja, and D. L. Griscom, *Defects in SiO₂ and Related Dielectrics: Science and Technology* (Springer, New York, 2000), p. 73.

³⁴S. Munekuni, T. Yamanaka, Y. Shimogaichi, R. Tohmon, Y. Ohki, K. Nagasawa, and Y. Hama, *J. Appl. Phys.* **68**, 1212 (1990).

³⁵A. F. Zatsepin, D. Y. Biryukov, and V. S. Kortov, *Latv. J. Phys. Tech. Sci.* **6**, 83 (2000), available at http://www.innovation.lv/fei-old/zurnals/content_6supp_2000.htm.

³⁶L. Skuja, B. Güttler, D. Schiel, and A. R. Silin, *J. Appl. Phys.* **83**, 6106 (1998).

³⁷R. Salh, “Defect related luminescence in silicon dioxide network: A review,” in *Crystalline Silicon - Properties and Uses*, edited by S. Basu (InTech, Rijeka, 2011), pp. 135–172.

³⁸D. L. Griscom, *Phys. Rev. B* **20**, 1823 (1979).

³⁹A. N. Trukhin, *Nucl. Instrum. Methods Phys. Res. B* **91**, 334 (1994).

⁴⁰A. N. Trukhin, *J. Non-Cryst. Solids* **149**, 32 (1992).

⁴¹A. Podhorodecki, M. Nyk, J. Misiewicz, and W. Strek, *Proc. SPIE* **6321**, 63210 (2006).

⁴²J. Schwartz, S. Aloni, D. F. Ogletree, and T. Schenkel, *New J. Phys.* **14**, 043024 (2012).

⁴³J. Koike, D. M. Parkin, and T. E. Mitchell, *Appl. Phys. Lett.* **60**, 1450 (1992).

⁴⁴A. Zanatta, A. Khan, and M. Kordesch, *J. Phys.: Condens. Matter* **19**, 436230 (2007).

⁴⁵S. Baranovski, *Charge Transport in Disordered Solids with Applications in Electronics* (Wiley, Chichester, England, 2006).